Structural Monitoring and Maintenance, *Vol. 8, No. 1 (2021) 69-90*
DOI: https://doi.org/10.12989/smm.2021.8.1.069

Active interface debonding detection of a Concrete Filled Tube (CFT) column by modal parameters and Continuous Wavelet Transform (CWT) technique

Adel Younesi [1a], Omid Rezaifar[*1], Majid Gholhaki [1b] and Akbar Esfandiari [2c]

[1] *Department of Civil Engineering, Semnan University, Semnan, Iran*
[2] *Department of Maritime Engineering, Amir Kabir University, Turkey*

(*Received August 6, 2020, Revised November 18, 2020, Accepted December 3, 2020*)

Abstract. In recent years, damage detection methods have been significantly increased in civil and mechanical structures. One of the most widely used and relatively new methods of signal processing is the method based on wavelet transform; with the help of this powerful tool, the damage in the structures can be detected in the early stages of damage formation, in order to prevent a larger damage event. In this paper, we have investigated the debonding damage of active surfaces in Concrete-Filled Tube (CFT) columns, which greatly reduces the effect of enclosure on concrete and decreases the bearing capacity of these tubes with the help of wavelet transformation (Discrete Wavelet Transform and Continuous Wavelet Transform). The debonding damage of the active surfaces was evaluated using wavelet types, and the occurrence and location of the damage were detected based on variations in frequency and mode shapes. The above studies have been done for the first six modes of the CFT column. The results of the analyzes indicate that the wavelet transform tool is very capable of detecting the occurrence and location of the damage and is able to detect high-level debonding damage in one side of the column that creates curvature and slight jump in the shape of the mode.

Keywords: damage detection; CFT column; active interface debonding; wavelet transform; modal analysis

1. Introduction

Concrete Filled Tube (CFT) columns are used gradually more and more as one of the main structural elements for resisting both vertical and lateral loads in multistory and tall building columns due to their advantages compared to circular CFT columns such as: (1) the cross-section shape agreeing well with the design need of the architecture plane of buildings; (2) more convenient construction measures at beam–column joints resulting in easy connection and less cost; (3) large moment of inertia of cross-section which leads to higher capacity of resisting lateral load. However, the axial load-bearing capacity of square CFT columns is lower than that of circular

*Corresponding author, Associate Professor, E-mail: orezayfar@semnan.ac.ir
[a] Ph.D. Graduate
[b] Associate Professor
[c] Associate Professor

 ISSN: 2288-6605 (Print), 2288-6613 (Online)

CFT columns because of the little effect of concrete confinement (Cai and He 2006, Rezaifar and Younesi 2017, 2016, Rezaifar *et al*. 2016, Younesi *et al*. 2019, 2020).

Analyzed shear-resistant capacity and the inner force transmission in steel-reinforced concrete T-shaped column-beam joints. It is found that the steel-reinforced concrete T-shaped column-reinforced concrete beam joint performs well under seismic conditions; moreover, shear-resistant capacity, ductility, and reliability are satisfactory. Conclusions derived from this research are useful for engineering practice (Xiang *et al*. 2017). In order to fulfil energy dissipation requirements, diagonal angle steel crosses are placed at the end of the steel truss. Specimens are designed based on different key parameters, including axial compression ratio and dimensions of chord, web and angle steels. It is found that a large steel ratio will generally increase the bearing capacity. However, a relatively high axial compression ratio will benefit the bearing capacity of joints, but has adverse effects on hysteresis behaviours. Further, some conclusions are drawn on the overall seismic performances of this type of joint (Deng *et al*. 2018).

Damage in a structure produces variations in its geometric and physical properties, which can result in changes in its natural frequencies and mode shapes. In the last years, several researchers have developed many damage detection methods based on dynamic parameters. Damage detection using wavelet transform is a recent area of research in structural health monitoring. Wavelet-based methods do not require the analysis of the complete structure and neither do they require any knowledge of the material properties nor the prior stress states of the structure. Although studies have shown that wavelet techniques are highly feasible for damage detection (Stubbs and Osegueda 1990, Chui 1992, Daubechies 1992, Schumaker and Webb 1994, Newland 1994, Wang and McFadden 1996, Wang and Deng 1999), the behaviors presented are rather fundamental and some specific issues have not been addressed.

A method for structural damage identification based on Chaotic Artificial Bee Colony (CABC) algorithm is presented by Xu *et al*. (2015a) ABC is a heuristic algorithm with simple structure, ease of implementation, good robustness but with slow convergence rate. To overcome the shortcoming, the tournament selection mechanism is chosen instead of the roulette mechanism and chaotic search mechanism is also introduced. Residuals of natural frequencies and Modal Assurance Criteria (MAC) are used to establish the objective function, ABC and CABC are utilized to solve the optimization problem. Two numerical examples are studied to investigate the efficiency and correctness of the proposed method. The simulation results show that the CABC algorithm can identify the local damage better compared with ABC and other evolutionary algorithms, even with noise corruption (Xu *et al*. 2015a). Research by Kwon (Kwon *et al*. 2008) is exploring a new method to damage detection in continuous structures using successive zooming genetic algorithm. Presented method is a kind of pseudo-discrete-variable-algorithm that counts the soundness variables as one (perfectly sound) if they are above a certain standard, such as 0.99. (Kwon *et al*. 2008).

An adaptive-scale damage detection strategy based on a wavelet finite element model (WFEM) for thin plate structures is established in He and Zhu, study. Equations of motion and corresponding lifting schemes for thin plate structures are derived with the tensor products of cubic Hermite multi-wavelets as the elemental interpolation functions (He and Zhu 2015). In Yazadanpanah's study, a new damage indicator based on mode shape data is introduced to identify damage in beam structures. In order to construct the indicator proposed, the mode shape, mode shape slope and mode shape curvature of a beam before and after damage are utilized (Yazdanpanah and Seyedpoor 2015).

A simply structural damage detection software is developed to identification damage in beams.

According to linear fracture mechanics theory, the localized additional flexibility in damage vicinity can be represented by a lumped parameter element. The damaged beam is modeled by wavelet based elements to gain the first three frequencies precisely (Xiang *et al*. 2011).

Considering the importance of CFT columns in high-rise buildings and other structures and the importance of identifying damage in CFT columns, some studies have been recently carried out by various researchers. In this section, studies have been conducted on troubleshooting reinforced concrete, steel and CFT columns.

Damage assessment of Reinforced Concrete (RC) columns retrofitted by advanced composite jackets was experimentally and analytically studied. The frequencies and mode shapes of the columns determined from the vibration tests and computed on the basis of the estimated stiffness showed excellent agreement. Pertinent to the purpose of the study is the success of quantification of the extent and location of stiffness degradation due to different levels of damage. Degradation of the shear stiffness as well as the flexural stiffness in the lap splice region, especially in the 1-in. unwrapped gap portion, of the column was a key parameter to represent the damage (Feng and Bahng 1999). A Bayesian probabilistic approach for damage detection has been proposed for the continuous monitoring of civil structures (Sohn and Law 1997). The proposed damage detection method was able to locate the damaged region using a simplified analytical model and the modal parameters estimated from the vibration tests, although (1) only the first bending and first torsional modes were estimated from the experimental test data, (2) the locations where the accelerations were measured did not coincide with the degrees of freedom of the analytical model, and (3) there existed discrepancies between the undamaged test structure and the analytical model. The Bayesian framework was able to systematically update the damage probabilities when new test data became available. Better diagnosis was obtained by employing multiple data sets than just by using each test data set separately (Sohn and Law 2000). In this paper, vibration based damage detection techniques were employed to detect damage in reinforced concrete column after different levels of quasi-static cyclic loadings. Results show that the identified damage is consistent with the observed damage in the composite beam (Xu and Gong 2010). In Moslehy *et al*.'s paper, an innovative piezoceramic-based approach is developed for the structural health monitoring of reinforced concrete columns. An innovative piezoceramic-based device, the smart aggregate, is utilized as a transducer for the health monitoring purpose. The proposed smart aggregate-based approach successfully evaluated the health status of concrete columns during the loading procedure. Sensor energy plots and 3-D normalized sensor energy plots demonstrated that the damages inside attenuated the transmitted energy. Wavelet-packet-based damage index and sensor history damage index evaluate the damage development in concrete columns under cyclic loading (Moslehy *et al*. 2010).

The interface device is a thin-walled beam-like member with a PZT patch mounted on it. A partial free surface in the bottom of the interface is intentionally designed to make the PZT patch freely vibrating and also allow to predetermine effective frequency ranges in the impedance-based technique. The implementation of the PZT-interface was successful in indicating various tension-losses in tendon anchorage systems with sensitive frequency bands below 100 kHz (Huynh *et al*. 2015). These conditions may cause decrement of bolt preload or even loosening of bolt. As a result, load carrying capacity of the connection is reduced and the structure could be collapsed. Therefore, to reduce maintenance costs and to increase the reliability of structures, the structural condition of such structural connections should be accurately assessed using appropriate local structural health monitoring (SHM) techniques during their lifetime (Li *et al*. 2014, 2016, Nagarajaiah and Erazo 2016, Kim *et al*. 2016).

A two-stage eigen-sensitivity based finite element (FE) model updating procedure is developed for structural parameter identification and damage detection for the IASC-ASCE structural health monitoring benchmark steel structure on the basis of ambient vibration measurements. Comparisons between the FE model updated results and the experimental data show that the eigen-sensitivity based FE model updating procedure is an effective tool for structural parameter identification and damage detection for steel frame structures (Wu and Li 2006). The paper, through the discussion of an experimental investigation, considers a combined approach based on artificial neural networks and genetic algorithms for structural damage identification. Results of the experimentation (where damage was known as both location and extent) were compared with the results of the optimization algorithm in order to verify its ability to match the actual damage (Betti *et al*. 2015).

In Xu *et al*. (2013) study, an active interface condition monitoring approach for CFST by the use of lead zirconate titanate (PZT) piezoceramics based functional smart aggregates (SAs) embedded in concrete as actuator and PZT patches bonded on the surface of the steel tube as sensors is proposed and verified experimentally. Analysis on the sensitivity of the two evaluation indices shows that the indices based on wavelet packet analysis are more sensitive to the debonding defect. The proposed PZT based active debonding monitoring method provides an innovative approach to detect the debonding damage of CFST columns (Xu *et al*. 2013). In addition, Xu *et al*. (2015a) are presented a PZT based active interface debonding defect detection approach for multi-chamber SRC columns and validated experimentally with an irregular multi-chamber SRC specimen. A number of embedded piezo-based functional elements (EPFEs) installed close to the steel plates and piezoelectric ceramic (PZT) patches bonded on the surface of the steel plates are used as actuators and sensors respectively. Results show that the amplitude and the wavelet packet energy of the measurement of the PZT sensors in the debonding region are obviously less than in the bonding region. The proposed approach provides a useful way for the interface debonding defect detection of large-scale irregular multi-chamber SRC members in super high-rise buildings (Xu *et al*. 2015a).

A number of researches studied about the behavior analysis and early warning of girder deflections of a steel-truss arch railway bridge under the effects of temperature and trains, Live-load strain evaluation of the prestressed concrete box-girder bridge using deep learning and clustering and Digital modeling on the nonlinear mapping (Zhao *et al*. 2019, 2020a, b).

In the present study, the existence and location of the debonding damage of active interface were investigated through the wavelet transforms. Accordingly, wavelet types were used to identify the defect, and the effect of wavelet type and defect position on the identification of damage was studied. In addition, the effect of the number of modes has also been evaluated. MATLAB and ABAQUS softwares have been used to extract and analyze the modal data, respectively.

2. Wavelet transform technique

Wavelet transform is a mathematical tool that converts a signal into a different form (as shown in Fig. 1) in order to reveal the characteristics of the original signal and represent the original signal more succinctly (Gao and Yan 2010, Debnath and Shah 2002, Mallat 2008). Important and widely used wavelet transform methods are: Continuous Wavelet Transform (CWT), Discrete Wavelet Transform (DWT) and Wavelet Packet Transform (WPT). In this research, CWT and

DWT have been considered.

2.1 Continuous Wavelet Transform(CWT)

The wavelet transform of a signal x(t) is calculated using Eq. (2), in which, the signal is compared with a set of template functions $\left(\psi_{s,\tau}(t)\right)$ obtained from the scaling (i.e., dilation and contraction) and shifting (i.e., translation along the time axis) of a base wavelet $\psi(t)$ and looking for their similarities.

The base wavelet is a small wave that has an oscillating wavelike characteristic and has its energy concentrated in time (Gao and Yan 2010, Mallat 2008).

$$\psi_{s,\tau}(t) = \frac{1}{\sqrt{s}}\psi\left(\frac{t-\tau}{s}\right) \tag{1}$$

$$wt(s,\tau) = \langle x(t), \psi_{s,\tau}\rangle = \frac{1}{\sqrt{s}}\int_{-\infty}^{+\infty} x(t)\psi^*\left(\frac{t-\tau}{s}\right)dt \tag{2}$$

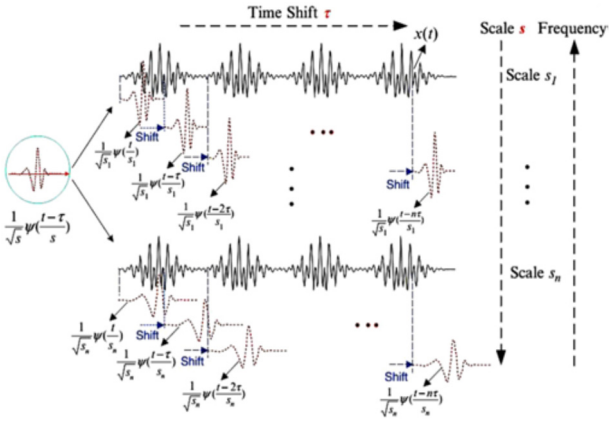

Fig. 1 Illustration of Wavelet transform (Gao and Yan 2010)

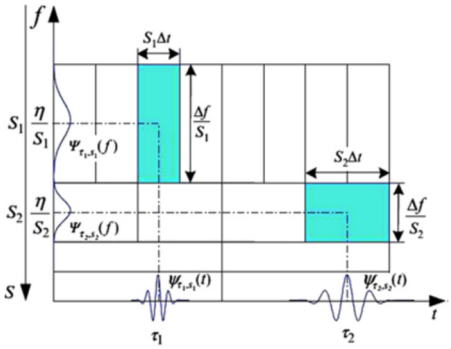

Fig. 2 Time and Frequency Resolutions of the Wavelet Transform (Gao and Yan 2010)

Where the symbol $s > 0$ represents the scaling parameter, which determines the time and frequency resolutions of the scaled base wavelet $\psi(t - (\tau/s))$. The specific values of s are inversely proportional to the frequency. The symbol τ is the shifting parameter, which translates the scaled wavelet along the time axis. The symbol * denotes the complex conjugation of the base wavelet $\psi(t)$ (Gao and Yan 2010, Mallat 2008).

As the wavelet contains two parameters, transforming a signal with the wavelet basis means that such a signal will be projected into a 2D, time-scale plane. Furthermore, because of the localization nature of the wavelet, the transformation will extract features from the signal in the time-scale plane that are not revealed in its original form.

2.2 Discrete Wavelet Transform (DWT)

Because of continuously variation of the scale and translation parameters, (s, τ), performing the Continuous Wavelet Transform (CWT) on a signal will lead to the generation of redundant information. This issue will increase the computational time and memory size. So, redundancy reduction in the wavelet coefficients among different scales is desired as much as possible. A way to reducing redundancy is to use a logarithmic discretization of the scales s and then link it values of translation parameter (Mallat 2008).

$$\begin{cases} s = s_0^j & s_0 \langle 1, j \in Z \\ \tau = k\tau_0 s_0^j & \tau_0 \neq 0, k \in Z \end{cases} \tag{3}$$

By assuming $s_0 = 2$ and $\tau_0 = 1$, the discrete wavelet transform of a given signal $x(t)$ is obtained using Eq. (4) (Gao and Yan 2010, Mallet 2008).

$$wt(j,k) = \langle x(t), \psi_{j,k} \rangle = \frac{1}{\sqrt{2}} \int_{-\infty}^{+\infty} x(t)\, \psi^* \left(\frac{t - k2^j}{2^j} \right) dt \tag{4}$$

If a set of wavelet coefficients, $\langle x(t), \psi_{j,k} \rangle$, exists that describes complete information of the signal $x(t)$, then the following statements must hold

$$A\|x(t)\|^2 \leq \sum_{j,k} \left| \left\langle x\left((t), \psi_{j,k}\right) \right\rangle \right|^2 \leq B\|x(t)\|^2, \qquad A, B \in R^+ \tag{5}$$

Where A and B are real positive numbers. In such a case, the signal $x(t)$ can be reconstructed through the inverse discretized wavelet transform.

$$x(t) = \frac{2}{A+B} \sum_{j=-\infty}^{\infty} \sum_{j=-\infty}^{\infty} wt(j,k) \psi_{j,k}(t) \tag{6}$$

2.3 Multi Resolution Analysis (MRA)

Fig. 3 shows a MRA, schematically. In MRA, a given signal can be decomposed in two parts,

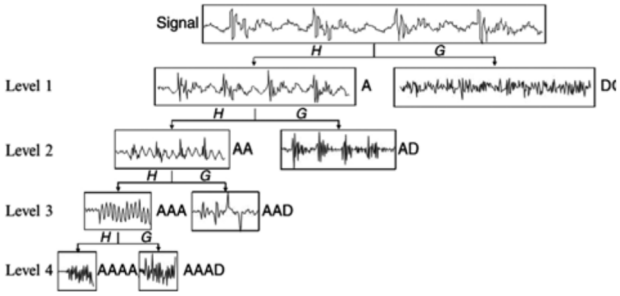

Fig. 3 Schematically Signal Decomposition using DWT (Gao and Yan 2010)

detailed and approximate information. Approximate information can be further decomposed to get the next level of detailed and approximate information. Such a decomposition process can be repeated until the designed scale j is reached. This is how a DWT is implemented. Equation 7 and 8 give detailed and approximate information in j scale (Gao and Yan 2010, Mallat 2008).

$$x_a^j = \sum_k a_{j,k}\varphi_{j,k} = \sum_k \langle x(t), \varphi_{j,k}(t)\rangle \varphi_{j,k}(t), \qquad k = z \tag{7}$$

$$x_a^j(t) = \sum_k d_{j,k}\psi_{j,k} = \sum_k \langle x(t), \psi_{j,k}(t)\rangle \psi_{j,k}(t), \qquad k = z \tag{8}$$

Where $a_{j,k}$ and $d_{j,k}$ are approximate and detailed coefficient, respectively. Consequently, a given signal can be decomposed into a set of subspace using Eq. (9).

$$x(t) = \sum_{j=-\infty}^{\infty}\sum_{j=-\infty}^{\infty} d_{j,k}\,\psi_{j,k}(t) + \sum_{k=-\infty}^{\infty} a_{j,k}\varphi_{j,k}(t) \tag{9}$$

Where J is a predetermined scale parameter. In above equations, $\varphi(t)$ is the scale function. For given signal, translation of wavelet is limited to length of $x(t)$ since zero frequency could not be covered in this situation, the scale function is used. $\varphi_{j,k}(t) = 2^{-j/2}\varphi(2^{-j}t - k)$ is the translated and scaled version of $\varphi(t)$ (Gao and Yan 2010).

2.4 Wavelet Packet Transform (WPT)

Discrete wavelet transform suffers from a relatively low resolution in the high-frequency region. The Wavelet Packet Transform (WPT), in comparison, decomposes the detailed information of the signal in the high-frequency region (Fig. 4), thereby overcoming this limitation (Gao and Yan 2010). The WPT is defined as follow (Gao and Yan 2010, Shao *et al*. 2014, Wang *et al*. 2014)

$$\begin{cases} u_{2n}^{(j)}(t) = \sqrt{2}\sum_k h(k)u_n^{(j)}(2t-k) & n = 0,1,2,\ldots \\ u_{2n+1}^{(j)}(t) = \sqrt{2}\sum_k g(k)u_n^{(j)}(2t-k) & n = 0,1,2,3,\ldots,m \end{cases} \tag{10}$$

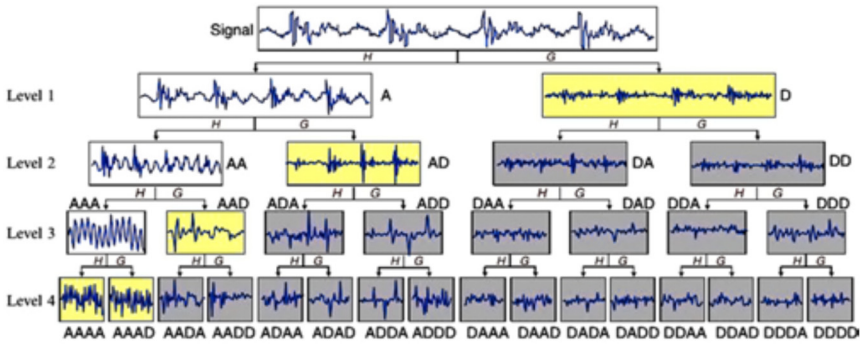

Fig. 4 Schematically Signal Decomposition using WPT (Gao and Yan 2010)

Where $u_0^{(0)}(t)$ is the scaling function, $u_0^{(0)}(t) = \varphi(t)$, and $u_1^{(0)}(t)$ is the base wavelet function, $u_1^{(0)}(t) = \psi(t)$. The superscript (j) denotes the j-th level wavelet packet basis, and there will be $2^j 2$ wavelet packet bases at the j-th level.

3. Introducting models and test conditions

3.1 Geometry of models

A concrete-filled tube square column with 800 mm length, 120 mm cross section, and 3 mm plate thickness were used in this study. The mechanical properties of concrete and steel are presented in Table 2.

3.2 Materials properties

The materials used in this study are steel and concrete. The mechanical properties of the materials are presented in Table 1.

Table 1 Material properties

Materials	$f_y(MPa)$	$f_u(MPa)$	$f_c^{`}(MPa)$	$E(10^3 MPa)$	ϑ	Specific gravity (MPa)
Steel	2400	3700	-	200	0.3	78.55
Concrete	-	-	245	24.7	0.2	21.70

Table 2 Introduction of models

Model	Sections size (mm)	Length (mm)	Type of model	Damage size (mm)	Damage location
H00000	120×120×3	800	Health	400×60	None
DM40×6	120×120×3	800	Damaged	400×60	Middle
DB40×6	120×120×3	800	Damaged	400×60	Bottom
DT40×6	120×120×3	800	Damaged	400×60	Top

3.3 Summary of models

The models examined include one healthy model and three faulty (damaged) models with debonding. These damages have been created in a particular side at different points of the column (high, middle and low) at 400 × 60 mm. Fig. 5 and Table 2 show the properties of the models under study.

The bottom of all models is fixed and the top is totally free and has the ability to move (cantilever column).

3.4 Test setup and instrumentation

Since the existence of any supporting conditions causes high rigidity in the structure and in order to stimulate it for modal analysis, great force is needed and this force may cause unforeseen damage and even collapse of the structure and error in the results will be analyzed on this basis, the present study has used free-free supporting conditions and to achieve this goal, the steel column is suspended by a high elastic cache and the accelerometer has been connected at one

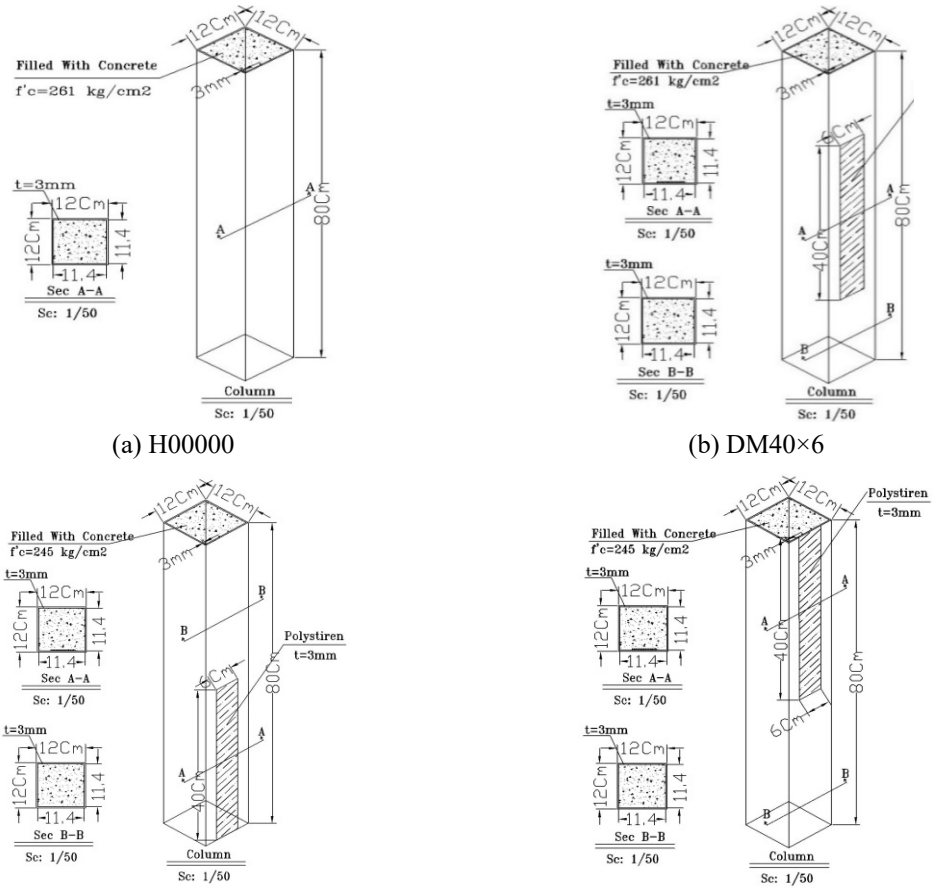

(a) H00000 (b) DM40×6

(c) DB40×6 (d) DT40×6

Fig. 5 Introduction of models and the location of their damage

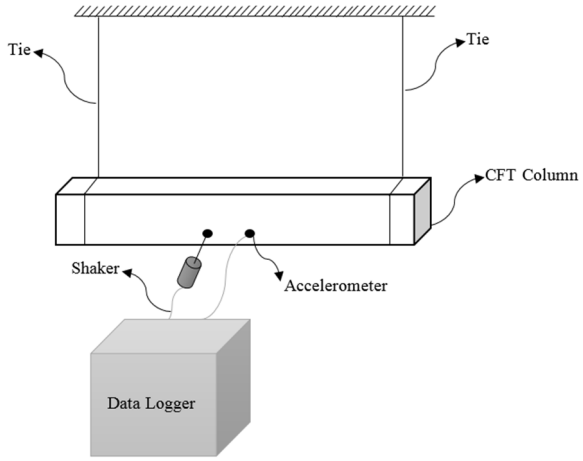

Fig. 6 Test set up

Table 3 The tools of tests

Equipment	Model	Manufacturer	Country of origin
Portable Pulse 4/2 I/O Module	3560C	B&K	Denmark
Accelerometer	4397	B&K	Denmark
Charge Convertor	2646	B&K	Denmark
Force Transducer	9301B	Kistler	Switzerland
Electrodynamic Shaker	TV51110-M	Tria	Germany
Power Amplifier	BAA120	Tira	Germany

point of the column (Fig. 6). The accelerometer sensor connection is located between the middle and the edges of the beam therefore first, it does not separate while the impact, and secondly, it is at zero point of the moment to have the least error. In the next step, the impact (Shaker) is applied to the test points (the nodes of the meshes) and for each impact, the frequency response function has been extracted, finally, by applying the shock and transferring it to the data logger and using the sum of the resulting frequency functions, and solving the differential equation, the frequencies and the known modes are obtained. The type of impact signal is selected so that non-linear effects of the specimen are averaged and the best linear model are presented. Choosing the best type of impact depends on the geometry and structure of the piece. Finding the best method does not follow the general rule and is achieved by trial and error.

The tools for testing are presented in Table 3.

3.5 Experimental verification

For verification of theoretical studies it has been done a test in the lab for intermediate debonding damage with Free-Free boundary condition, and the theoretical studies are developed based on the results of this test. Set-up testing and test samples are provided in Fig. 7. According to Fig. 7 for test, the specimen has been suspended by drawstring and it Stimulated by Shaker.

(a) DB40×6 test specimen

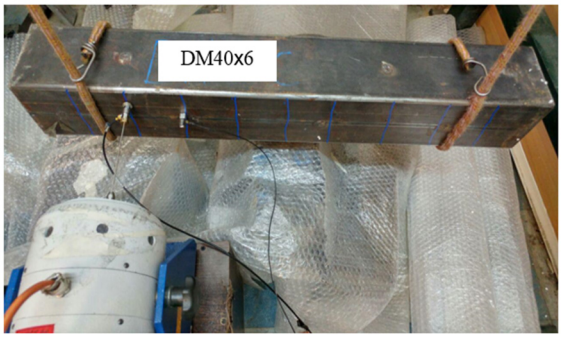

(b) Test set up

Fig. 7 Test specimen and set up

4. Finite element modeling

ABAQUS6.13 software has been used for the finite element modeling. Solid and shell elements are used in the finite element modeling for concrete solid and steel, respectively. Steel and concrete are frictionally connected with a coefficient of 0.6, and at the debonding surfaces, this coefficient is considered to be zero, so that the debonding defect can be simulated precisely.

Accordingly, the analysis has been done on mesh size, and the size of the mesh has been

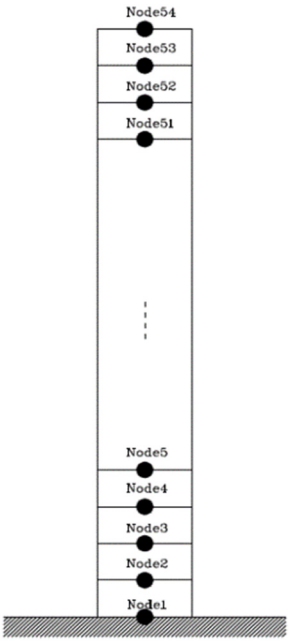

Fig. 8 Analytical Model of columns

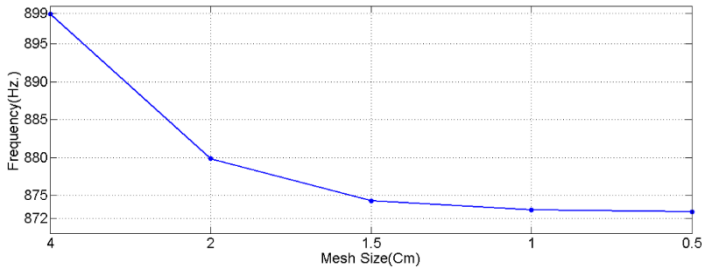

Fig. 9 Effect of mesh size at frequency

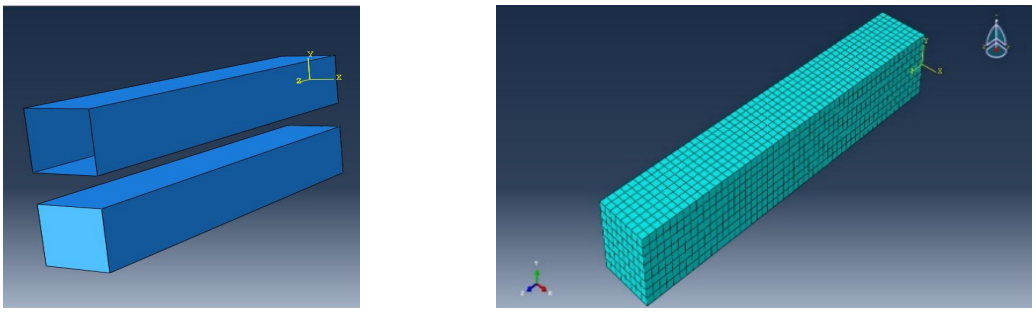

Fig. 10 Details of modeling in ABAQUS software

reduced to minimize the size of the mesh, no noticeable change in the results. The size of the mesh in this research was determined to be 1.5 cm. Fig. 9 shows the frequency for different mesh sizes. According to the Fig. 10, no changes in the frequencies have been made from mesh sizes less than 1.5 cm, but the analysis time has been very long. As in the 0.5 cm mesh, the program needs to analyze about 107,000 meshes that are time consuming. Given the size of the mesh in the experimentally specimens for data acquisition is 40 mm. First, the size of the mesh is selected in the modeling of 40 mm, then the size of the mesh is reduced so that there is not much change in frequency and do not prolong the analysis time.

5. Results and discussion

For damage detection, the mode shapes (Figs. 11(a), (b) and (c)) and the frequency (Table 4) of the specimen is extracted and the location of the damage has been identified using the wavelet transform.

The reason for the difference in the appearance of experimental and theoretical modes is that in the experimental mode, data is extracted from several points along the column, but in the theoretical model, the column is assumed to be integrated. On the other hand, the materials in the experimental model are more uniform than the experimental specimen. Another reason for this difference is the presence of laboratory noise.

5.1 Modal values

The absolute values of the frequency and the frequency difference of the damaged models

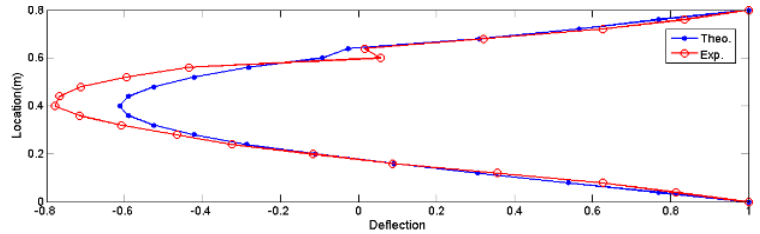

(a) Mode I

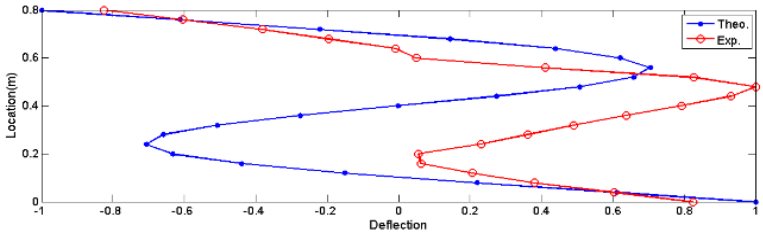

(b) Mode II

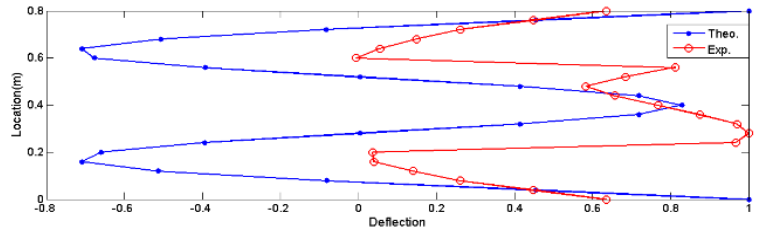

(c) Mode III

Fig. 11 Comparison of the experimental and theoretical mode shapes of DM40×6 Specimen

Table 4 Frequency of specimens (Rad/Sec.)

Model type	Mode1	Mode2	Mode3
Theoretical	788.23	1556.3	2611.7
Experimental	756.82	1498.5	2571.6
Difference (%)	4.15	3.86	1.56

Table 5 Frequency of models (Hz.)

Model	H00000(F)	DM40×6(Fi)	Fi-F	DB40×6(Fj)	Fj-F	DT40×6(Fk)	Fk-F
1	44.212	42.814	-3.1620	42.814	-3.1620	44.203	-0.0204
2	44.212	42.829	-3.1281	43.418	-1.7959	44.211	-0.0023
3	237.29	235.86	-0.6026	226.42	-4.5809	237.26	-0.0126
4	243.46	237.35	-2.5096	237.46	-2.4645	243.23	-0.0945
5	243.46	237.6	-2.4070	239.77	-1.5156	243.45	-0.0041
6	385.35	380.75	-1.1937	381.19	-1.0795	385.33	-0.0052
7	589.58	577.27	-2.0879	578.12	-1.9438	587.64	-0.3291

Table 5 Continued

Model	H00000(F)	DM40×6(Fi)	Fi-F	DB40×6(Fj)	Fj-F	DT40×6(Fk)	Fk-F
8	589.58	579.57	-1.6978	582.25	-1.2433	589.54	-0.0068
9	711.48	707.13	-0.6114	681.27	-4.2461	711.26	-0.0309
10	992.37	970.93	-2.1605	970.21	-2.2330	982.18	-1.0268
11	992.37	981.37	-1.1085	982.10	-1.0349	992.22	-0.0151
12	1149.3	1135.4	-1.2094	1132.6	-1.4531	1148.7	-0.0522
13	1184.5	1177	-0.6332	1137.2	-3.9932	1183.7	-0.0675
14	1423.7	1263.7	-11.238	1348.4	-5.2890	1270.2	-10.782
15	1423.7	1286	-9.6720	1409.7	-0.9834	1274.1	-10.508

compared to the healthy model for the first 15 modes are presented in Table 5.

The results show that the damage caused the reduction of frequencies in all the modes. The mode shapes of all models are shown in Figs. 12(a) to 9(f).

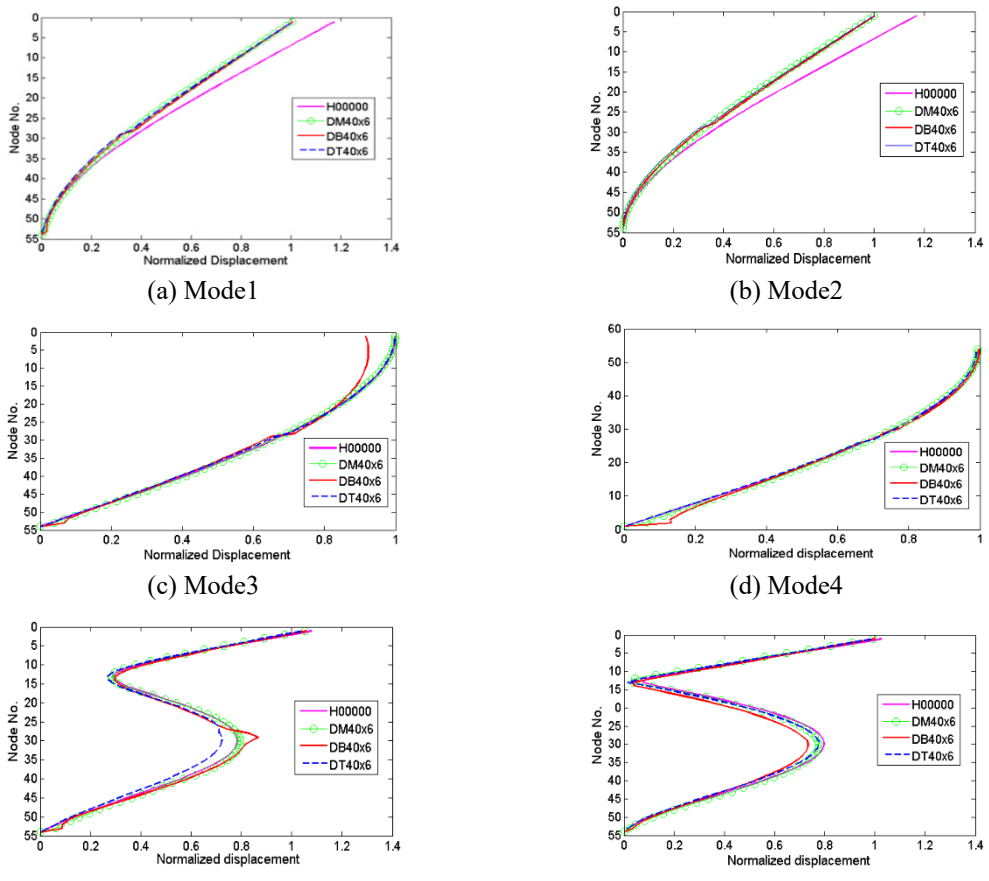

(a) Mode1 (b) Mode2

(c) Mode3 (d) Mode4

(e) Mode5 (f) Mode6

Fig. 12 Comparison of the theoretical models' mode shapes

As shown in Fig. 9, the debonding damage causes changes in the mode shape values along the structure and discontinuity (jump) in the mode shape can be seen at the starting points of the debonding, but these slight changes in the mode shape are not easily recognizable.

5.2 Damage detection

5.2.1 Detecting the existence of damage

One way for detection of damage existence in structures is the MAC. The MAC value of eigenvectors is used to compare the mode shapes of the undamaged and damaged structures, and is given by

$$MAC\left(\varphi_i^T, \tilde{\varphi}_i\right) = \frac{\left|\varphi_i^T \tilde{\varphi}_i\right|^2}{\left(\varphi_i^T \varphi_i\right)\left(\tilde{\varphi}_i^T \tilde{\varphi}_i\right)} \tag{11}$$

Where φ_i represents the i-th eigenvector of the undamaged structure, and $\tilde{\varphi}_i$ that with the damaged structure. One way to detect the existence of damage in the structure is the MAC method. In Table 6, MAC values and the frequencies of the first 6 mode shapes are presented and their differences are compared to the healthy model.

The comparative chart for MAC values is also shown in Fig. 13. According to Table 6, the frequency in all modes is reduced due to the damage caused compared to the healthy model, which indicates the existence of damage. On the other hand, MAC values in all modes are less than one as a result of the damage, indicating the inconsistency of the mode shape of the healthy and damaged structures. According to Eq. (11), the value of one indicates the complete conformance of the mode shapes, and the zero value represents the non-conformance and perpendicularity of the vectors of the mode shape compared to each other. Greater distance of this value from the value of one leads to less conformance of the modes indicating the existence of damage.

Table 6 Natural frequencies of the first 6 mode shapes of all models and MAC values

Model	MAC & Freq.	Mode1 = 44.212 Hz	Mode2 = 44.212 Hz	Mode3 = 237.29 Hz	Mode4 = 243.46 Hz	Mode5 = 243.46 Hz	Mode6 = 385.35 Hz
DM40×6	Freq.	42.814	42.829	235.86	237.35	237.60	380.75
	Diff. from the H00000	-3.16204	-3.12811	-0.60264	-2.50965	-2.40697	-1.19372
	MAC	0.999695	0.999919	0.999923	0.999229	0.999032	0.999736
DB40×6	Freq.	42.814	43.418	226.42	237.46	239.77	381.19
	Diff. from the H00000	-3.16204	-1.79589	-4.58089	-2.46447	-1.51565	-1.07954
	MAC	0.999647	0.999856	0.99893	0.997387	0.995008	0.999052
DT40×6	Freq.	44.203	44.211	237.26	243.23	243.45	385.33
	Diff. from the H00000	-0.02036	-0.00226	-0.01264	-0.09447	-0.00411	-0.00519
	MAC	0.999903	0.999833	0.999933	0.999275	0.999476	0.999946

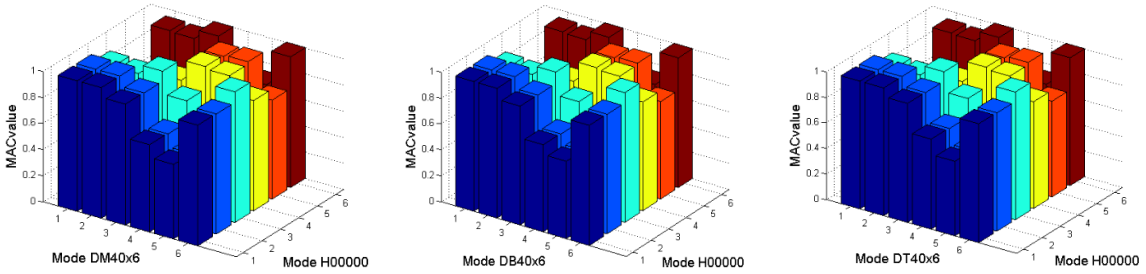

(a) DM40×6 (b) DB40×6 (c) DT40×6

Fig. 13 Bar chart of the models' MAC values

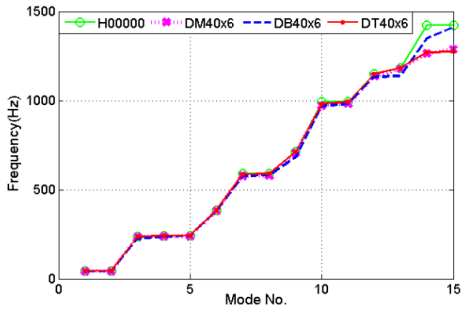

Fig. 14 The frequencies of models

According to Fig. 14, increasing the number of the mode leads to an increase in the frequency difference of the models. On the other hand, the frequency increase rate in 5 intermediate modes is more than 5 primary and end modes.

5.2.2 Damage localization by continuous wavelet transform

In order to detect the location of damage in structures, the mode shape extracted from ABAQUS is called in the MATLAB software, and different wavelets are applied to the first three modes (main modes of the structure). It is worth noting that it is more difficult to identify damage in low modes due to minor changes, but it is more accessible in real projects. Since more concentrated damage leads to more jump (variation) within the scope of damage, and it will be easier to detect, and in fact, a great amount of steel can surface is debonded from the concrete core, the dimensions of debonding have been considered large (about 25% of the column side). Fig. 15 presents the damage detection in the proposed models using Haar and db5 wavelet transformation with Level = 1 done in two modes of CWT and DWT.

According to Fig. 15, haar wavelet in CWT mode has accurately detected the location of the damage. Since debonding was artificially created at half of the column length, jump occurred at 1.4 and 3.4 points in the length of the column, indicating the discontinuity point. On the other hand, the DWT has been able to detect the zone of damage with less precision. As shown in Fig. 15(b), the starting point of discontinuity is precisely identified, but the endpoint is not detectable.

Similarly, in the DB40×6 model, the damage zone created at the foot of the column (length of 400 mm) was identified. As shown in Figs. 16(a) and 16(b), at the starting points of discontinuity (2.4 and 4.2 column length), jump has been created in the wavelet transform coefficient.

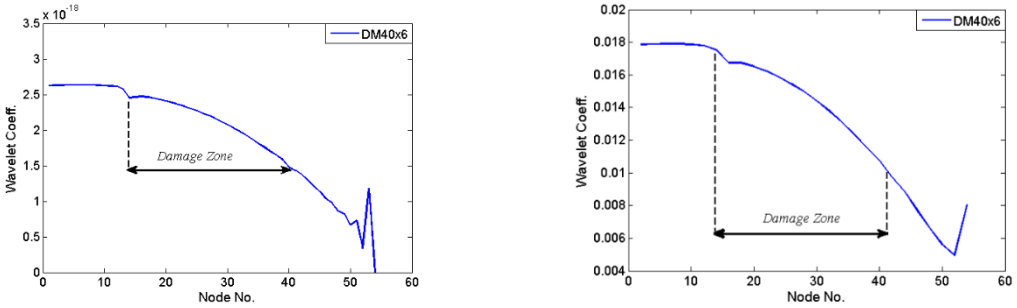

(a) CWT (b) DWT

Fig. 15 Detection of the debonding zone in DM40×6 by haar wavelet

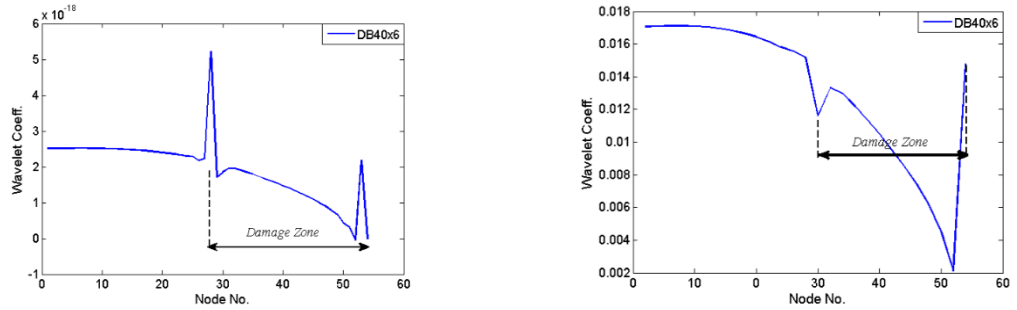

(a) CWT (b) DWT

Fig. 16 Detection of the debonding zone in BD40×6 by Haar wavelet

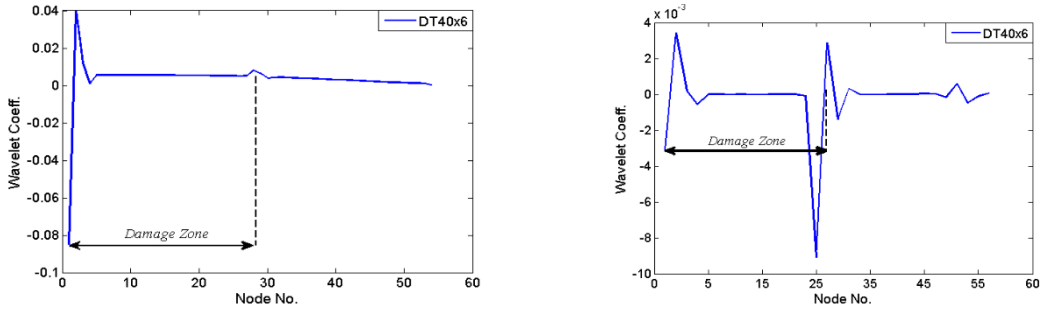

(a) CWT (b) DWT

Fig. 17 Detection the debonding zone in DT40×6 by db5 wavelet

In order to detect the damage in the DT40×6 model, Haar wavelet is not detectable due to the damage in the cantilever section of the column (above the column), so db5 wavelet has been used. In this wavelet, the midpoint of the positive and negative jumps represents the location of discontinuity (see Figs. 17(a) and 17(b)). On the other hand, since the start point of debonding is in the cantilever part, the wavelet recognizes this point as a large discontinuity point, which may cause some errors.

Table 7 Introduction of Wavelets used

Wavelet	Haar	DB1	Sym3	Coif1	Bior1.3	Dmey
Level	1	1	1	2	2	1

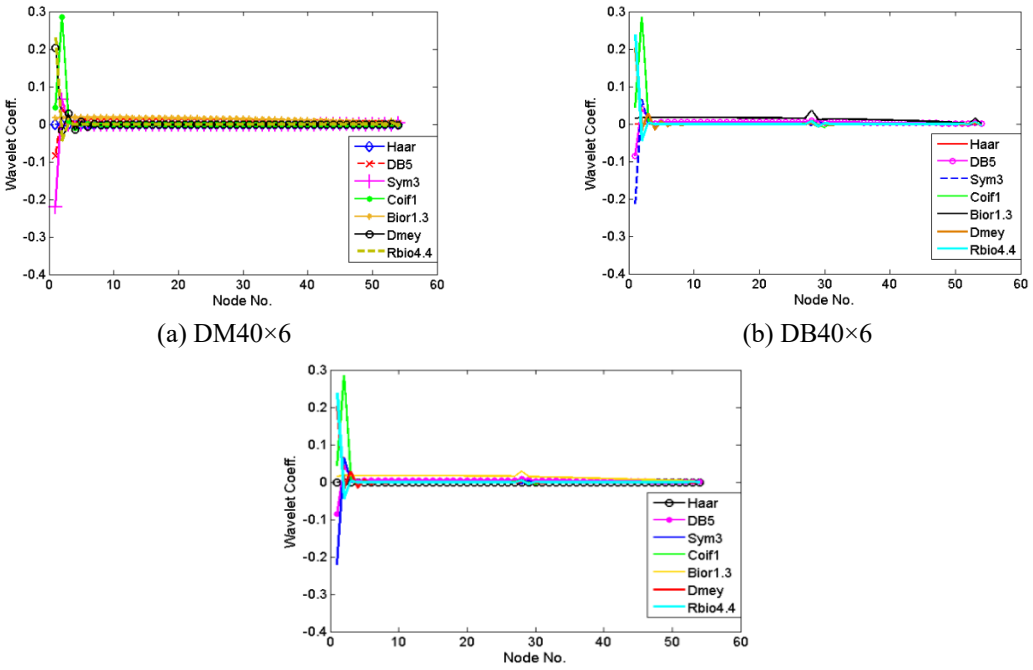

(a) DM40×6 (b) DB40×6

(c) DT40×6

Fig. 18 The effect of wavelet type in damage detection

5.2.3 Effect of wavelet type selection

In this section, the effect of wavelet type on the detection of debonding damage has been evaluated. To do this, the effects of the wavelets presented in Table 6 on the signal of the first mode of the DM40×6, DB40×6 and DT40×6 models have been compared (Table 7).

All wavelets have almost the same behavior in damage detection. In accordance with Figs. 16(a) to (c), the zone of damage is correctly detected in all wavelets. In Figs. 16(b), (c), the jump location is clearly indicated, which indicates the beginning of the discontinuity points (damage zone), but in Fig. 18(a), despite the fact that the damage zone is not clearly known, the extent of damage is correctly detected.

5.2.4 Effect of mode number

This section attempts to examine the effect of higher modes in detection in order to be considered in operational studies. In Fig. 19, this topic has been investigated for the first three modes of the damaged models.

In all models, the wavelet coefficient in higher modes is more than lowest modes, and the results indicate that damage in the higher modes is easier to detect than low modes.

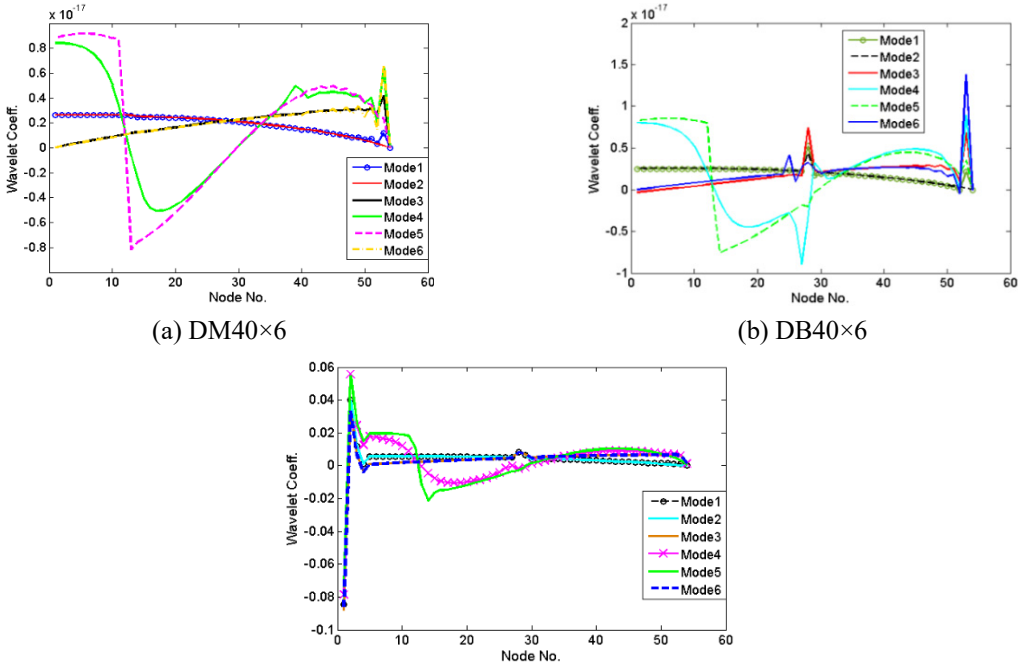

(a) DM40×6 (b) DB40×6

(c) DT40×6

Fig. 19 The effect of the mode number on damage detection

In the first modes (the main modes), the wavelet coefficient in the discontinuous points (beginning of damage or location of damage) is much lower than the higher modes and it is more difficult to detect the damage with these modes, but the low modes in laboratory studies or in troubleshooting real structures (buildings, dams, etc.) are more achievable. On the other hand, achieving higher modes requires a higher cost, and a higher impulse is needed to stimulate the structure and this force may damage the structure itself. Accordingly, in this study, the first mode is more evaluated.

6. Conclusions

Due to the population growth rate and the lack of urban space, there is more need to build a very high-rise building. For high-rise buildings, the columns used should occupy less space while maintaining a high resistance-weight ratio. CFT columns with such features are intended by designers and builders, accordingly, monitoring the health of these types of columns is examined in this study.

Regarding the studies done in troubleshooting of concrete-filled tube columns, it is concluded that the wavelet transform is a very powerful tool for damage detection, especially the CFT columns; it detects the damage correctly and with high precision. Wavelet types have also been studied in this research, in which all of the wavelets have been able to detect the location of the damage well.

The results show that debonding reduced the frequency of the structure, and on the other hand,

it made the MAC values less than one, confirming the damage to the structure. In addition, variations in the shape of the modes also prove damage. On the other hand, the results show that the higher modes are more sensitive to damage and damage detection is more easily possible, but the main modes (the first three modes) are less sensitive to damage, but are less expensive. In addition, the results show the method studied in this research can accurately determine the location of the damage and it is suitable for all types of columns. On the other hand, shape and position of damage do not affect the accuracy of the method.

Acknowledgments

The authors would like to thank ITRAC CO. for test of specimens and Mr. Bagher Sadeghi (MSc. graduate of structural engineering, Semnan University, Iran) for his contribution in preparing the numerical example of this paper.

References

Betti, M., Facchini, L. and Biagini, P. (2015), "Damage detection on a three-storey steel frame using artificial neural networks and genetic algorithms", *Meccanica*, **50**(3), 875-886. https://doi.org/10.1007/s11012-014-0085-9

Cai, J. and He, Z.Q. (2006), "Axial load behavior of square CFT stub column with binding bars", *J. Constr. Steel Res.*, **62**(5), 472-483. https://doi.org/10.1016/j.jcsr.2005.09.010

Chui, C.K. (1992), *An introduction to wavelets*, San Diego: Academic Press.

Daubechies, I. (1992), "Ten lectures on wavelets", Society for industrial and applied mathematics.

Debnath, L. and Shah, F.A. (2002), "Wavelet transforms and their applications", Boston: Birkhäuser, pp. 12-14.

Deng, Z., Hu, Q., Zeng, J., Xiang, P. and Xu, C. (2018), "Structural performance of steel-truss-reinforced composite joints under cyclic loading", *Proceedings of the Institution of Civil Engineers-Structures and Buildings*, **171**(2), 130-148. https://doi.org/10.1680/jstbu.16.00188

Feng, M.Q. and Bahng, E.Y. (1999), "Damage assessment of jacketed RC columns using vibration tests", *J. Struct. Eng.*, **125**(3), 265-271. https://doi.org/10.1061/(ASCE)0733-9445(1999)125:3(265)

Gao, R.X. and Yan, R. (2010), *Wavelets*: *Theory and applications for manufacturing*, Springer Science & Business Media.

He, W.Y. and Zhu, S. (2015), "Adaptive-scale damage detection strategy for plate structures based on wavelet finite element model", *Struct. Eng. Mech., Int. J.*, **54**(2), 239-256. https://doi.org/10.12989/sem.2015.54.2.239

Huynh, T.C., Lee, K.S. and Kim, J.T. (2015), "Local dynamic characteristics of PZT impedance interface on tendon anchorage under prestress force variation", *Smart Struct. Syst., Int. J.*, **15**(2), 375-393. https://doi.org/10.12989/sss.2015.15.2.375

Kim, J.T., Sim, S.H., Cho, S., Yun, C.B. and Min, J.Y. (2016), "Recent R&D activities on structural health monitoring in Korea", *Struct. Monit. Maint., Int. J.*, **3**(1), 91-114. https://doi.org/10.12989/smm.2016.3.1.091

Kwon, Y.D., Kwon, H.W., Kim, W. and Yeo, S.D. (2008), "Structural damage detection in continuum structures using successive zooming genetic algorithm", *Struct. Eng. Mech., Int. J.*, **30**(2), 135-146. https://doi.org/10.12989/sem.2008.30.2.135

Li, H.N., Yi, T.H., Ren, L., Li, D.S. and Huo, L.S. (2014), "Review on innovations and applications in structural health monitoring for infrastructures", *Struct. Monit. Maint., Int. J.*, **1**(1), 1-45. https://doi.org/10.12989/smm.2014.1.1.001

Li, H.N., Li, D.S., Ren, L., Yi, T.H., Jia, Z.G. and Li, K.P. (2016), "Structural health monitoring of

innovative civil engineering structures in Mainland China", *Struct. Monit. Maint., Int. J.*, **3**(1), 1-32. https://doi.org/10.12989/smm.2016.3.1.001

Mallat, S. (2008), *A Wavelet Tour of Signal Processing: The Sparse Way*, Academic, Burlington, Mass, p. 832.

Moslehy, Y., Gu, H., Belarbi, A., Mo, Y.L. and Song, G. (2010), "Smart aggregate-based damage detection of circular RC columns under cyclic combined loading", In: *Structures Congress 2010: Proceedings of the 19th Analysis and Computation Specialty Conference*, pp. 140-158.

Nagarajaiah, S. and Erazo, K. (2016), "Structural monitoring and identification of civil infrastructure in the United States", *Struct. Monit. Maint., Int. J.*, **3**(1), 51-69. https://doi.org/10.12989/smm.2016.3.1.051

Newland, D.E. (1994), "Wavelet analysis of vibration: part 2—wavelet maps".

Rezaifar, O. and Younesi, A. (2016), "Finite element study the seismic behavior of connection to replace the continuity plates in (NFT/CFT) steel columns", *Steel Compos. Struct., Int. J.*, **21**(1), 73-91. https://doi.org/10.12989/scs.2016.21.1.073

Rezaifar, O. and Younesi, A. (2017), "Experimental study discussion of the seismic behavior on new types of internal/external stiffeners in rigid beam-to-CFST/HSS column connections", *Constr. Build. Mater.*, **136**, 574-589. https://doi.org/10.1016/j.conbuildmat.2017.01.032

Rezaeifar, O., Younesi, A. and Gholhaki, M. (2016), "Seismic Retrofit of a Historical Building in Tehran University Museum Using FRP Technology and Steel Jacketing", *J. Rehabilit. Civil Eng.*, **4**(1), 41-54.

Schumaker, L.L. and Webb, G. (Eds.) (1994), *Recent advances in wavelet analysis*, Academic Press, **3**.

Shao, R., Hu, W., Wang, Y. and Qi, X. (2014), "The fault feature extraction and classification of gear using principal component analysis and kernel principal component analysis based on the wavelet packet transform", *Measurement*, **54**, 118-132. https://doi.org/10.1016/j.measurement.2014.04.016

Sohn, H. and Law, K.H. (1997), "A Bayesian probabilistic approach for structure damage detection", *Earthq. Eng. Struct. Dyn.*, **26**(12), 1259-1281. https://doi.org/10.1002/(SICI)1096-9845(199712)26:12<1259::AID-EQE709>3.0.CO;2-3

Sohn, H. and Law, K.H. (2000), "Bayesian probabilistic damage detection of a reinforced-concrete bridge column", *Earthq. Eng. Struct. Dyn.*, **29**(8), 1131-1152. https://doi.org/10.1002/1096-9845(200008)29:8<1131::AID-EQE959>3.0.CO;2-J

Stubbs, N. and Osegueda, R. (1990), "Global damage detection in solids- Experimental verification", *Int. J. Anal. Experim. Modal Anal.*, **5**, 81-97.

Wang, Q. and Deng, X. (1999), "Damage detection with spatial wavelets", *Int. J. Solids Struct.*, **36**(23), 3443-3468. https://doi.org/10.1016/S0020-7683(98)00152-8

Wang, W.J. and McFadden, P.D. (1996), "Application of wavelets to gearbox vibration signals for fault detection", *J. Sound Vib.*, **192**(5), 927-939. https://doi.org/10.1006/jsvi.1996.0226

Wang, Z., Bian, S., Lei, M., Zhao, C., Liu, Y. and Zhao, Z. (2014), "Feature extraction and classification of load dynamic characteristics based on lifting wavelet packet transform in power system load modeling", *Int. J. Elect. Power Energy Syst.*, **62**, 353-363. https://doi.org/10.1016/j.ijepes.2014.04.051

Wu, J.R. and Li, Q.S. (2006), "Structural parameter identification and damage detection for a steel structure using a two-stage finite element model updating method", *J. Constr. Steel Res.*, **62**(3), 231-239. https://doi.org/10.1016/j.jcsr.2005.07.003

Xiang, J., Jiang, Z., Wang, Y. and Chen, X. (2011), "Study on damage detection software of beam-like structures", *Struct. Eng. Mech., Int. J.*, **39**(1), 77-91. https://doi.org/10.12989/sem.2011.39.1.077

Xiang, P., Deng, Z.H., Su, Y.S., Wang, H.P. and Wan, Y.F. (2017), "Experimental investigation on joints between steel-reinforced concrete T-shaped column and reinforced concrete beam under bidirectional low-cyclic reversed loading", *Adv. Struct. Eng.*, **20**(3), 446-460. https://doi.org/10.1177/1369433216653841

Xu, B. and Gong, X. (2010), "Damage Detection of Reinforced Concrete Columns Based on Vibration Tests. In Earth and Space 2010: Engineering, Science", *Proceedings of the 12th Biennial International Conference on Engineering, Construction, and Operations in Challenging Environments*, pp. 2321-2329. https://doi.org/10.1061/41096(366)214

Xu, B., Li, B. and Song, G. (2013), "Active debonding detection for large rectangular CFSTs based on

wavelet packet energy spectrum with piezoceramics", *J. Struct. Eng.*, **139**(9), 1435-1443. https://doi.org/10.1061/(ASCE)ST.1943-541X.0000632

Xu, B., Shu, Z. and Dyke, S. (2015a), "Embedded Interface Debonding Detection for an Irregular Complex Multi-chamber Steel Reinforced Concrete Column with PZT Impedance", *Struct. Health Monitor.*

Xu, H.J., Ding, Z.H., Lu, Z.R. and Liu, J.K. (2015b), "Structural damage detection based on Chaotic Artificial Bee Colony algorithm", *Struct. Eng. Mech., Int. J.*, **55**(6), 1223-1239. https://doi.org/10.12989/sem.2015.55.6.1223

Yazdanpanah, O. and Seyedpoor, S.M. (2015), "A new damage detection indicator for beams based on mode shape data", *Struct. Eng. Mech., Int. J.*, **53**(4), 725-744. https://doi.org/10.12989/sem.2015.53.4.725

Younesi, A., Rezaifar, O., Gholhaki, M. and Esfandiari, A. (2019), "Structural health monitoring of a concrete-filled tube column", *Magaz. Civil Eng.*, **85**(1).

Younesi, A., Rezaeifar, O., Gholhaki, M. and Esfandiari, A. (2020), "Damage Detection in Concret Filled Tube Column Based on Exper-imentally Modal Data and Wavelet Technique", *Mech. Adv. Compos. Struct.* [In Press]

Zhao, H.W., Ding, Y.L., Nagarajaiah, S. and Li, A.Q. (2019), "Behavior analysis and early warning of girder deflections of a steel-truss arch railway bridge under the effects of temperature and trains: case study", *J. Bridge Eng.*, **24**(1), 05018013. https://doi.org/10.1061/(ASCE)BE.1943-5592.0001327

Zhao, H., Ding, Y., Li, A., Ren, Z. and Yang, K. (2020a), "Live-load strain evaluation of the prestressed concrete box-girder bridge using deep learning and clustering", *Struct. Health Monitor.*, **19**(4), 1051-1063. https://doi.org/10.1177/1475921719875630

Zhao, H., Ding, Y., Li, A., Sheng, W. and Geng, F. (2020b), "Digital modeling on the nonlinear mapping between multi-source monitoring data of in-service bridges", *Struct. Control Health Monitor.*, e2618. https://doi.org/10.1002/stc.2618

TY